Autocalibrated colloidal interaction measurements with extended optical traps

Marco Polin,* Yohai Roichman, and David G. Grier†
Department of Physics and Center for Soft Matter Research, New York University, New York, New York 10003, USA
(Received 16 November 2007; revised manuscript received 22 February 2008; published 1 May 2008)

We describe an efficient technique for measuring the effective interaction potential for pairs of colloidal particles. The particles to be tested are confined in an extended optical trap, also known as a line tweezer, that is projected with the holographic optical trapping technique. Their diffusion along the line reflects not only their intrinsic interactions with each other, but also the influence of the line's potential energy landscape and interparticle interactions mediated by scattered light. We demonstrate that measurements of the particles' trajectories at just two laser powers can be used to correct explicitly for optically induced forces and that statistically optimal analysis for optically induced forces yields autocalibrated measurements of the particles' intrinsic interactions with remarkably few statistically independent measurements of the particles' separation.

DOI: 10.1103/PhysRevE.77.051401 PACS number(s): 82.70.Dd, 87.80.Cc, 42.40.Jv, 05.40.Jc

Colloidal interactions tend to be diminutive, often no greater than a few femtonewtons, and typically are masked by vigorous Brownian motion. Nevertheless, they govern the microscopic stability and macroscopic properties of colloidal dispersions. Monitoring these interactions therefore is useful for understanding and controlling the many natural and industrial processes governed by colloidal dynamics.

This paper introduces an efficient and accurate method for measuring the interactions between a pair of colloidal particles that minimizes the measurement duration by optimizing the use of data. Combining optical micromanipulation [1], digital video microscopy [2–5], and a new analytical scheme based on adaptive kernel density estimation [6], this method requires just a few thousand measurements of the interparticle separation to characterize the pair potential of micrometer-scale particles in water. It also avoids experimental artifacts identified in previous studies of colloidal interactions and automatically separates the measured pair potential into intrinsic and optically induced contributions.

Section I reviews methods for measuring colloidal interactions with an emphasis on the practical considerations that have limited their widespread adoption. This section also highlights some of the benefits and challenges of confining colloidal particles to one dimension using extended optical traps known as line tweezers. Section II briefly describes our holographic implementation of line traps, which have been described in detail elsewhere [1,7]. The principal contributions of this paper are presented in Sec. III, which addresses the statistical mechanics of interacting colloidal particles on a line trap. This discussion develops a statistically optimal analysis of trapped particles' trajectories that yields accurate results for the pair potential with exceedingly small data sets. We apply these methods to a well-studied model system in Sec. IV to demonstrate that just 4000 statistically independent samples of two particles' trajectories can suffice to measure their pair potential to within $\pm 0.5 k_B T$.

I. MEASURING COLLOIDAL INTERACTIONS

Most methods for measuring colloidal interactions use digital video microscopy [2,4,8] to track particles' motions. They differ in how the particles are handled during the measurement and in how the pair potential is recovered from the measured trajectories. For instance, colloids' interactions can be inferred from the pair distribution function of dispersions in equilibrium. Imaging measurements of the distribution function [9–11] involve large numbers of particles with sufficiently uniform properties that interpreting the many-particle statistics in terms of an effective pair potential is meaningful. This approach is limited, therefore, to measuring interactions among identical particles and cannot be applied to heterogeneous samples. Acquiring sufficient statistics to measure interactions at small separations requires large data sets and long experimental runs [3]. Maintaining sufficiently uniform conditions over the courses of such a measurement can be challenging [12,13]. Increasing the particles' concentration to obtain results more quickly introduces many-body correlations that can obscure the pair potential [14,15]. Even imaging an equilibrium dispersion poses challenges because high-resolution microscopes have a limited depth of field [16,17], three-dimensional imaging techniques can be too slow to acquire snapshots of the particle distributions, and confining the particles to a plane can modify their interactions [5,18,19]. The images themselves can be subject to artifacts, identified in Ref. [4], that must be addressed with care to obtain meaningful results [4,5].

Many of the limitations and much of the time and difficulty involved in equilibrium interaction measurements can be avoided by using optical tweezers [20] to arrange pairs [21] or clusters [15] of particles into appropriate configurations. Colloidal interaction measurements based on optical tweezer manipulation generally fall into two categories: measurements performed with intermittent or blinking traps, and those performed with continuously illuminated traps. In the former case, particles positioned by optical tweezers are released by extinguishing the traps [18,21–23] and the resulting nonequilibrium trajectories can be analyzed with a Fokker-Planck formalism [21,23] to yield the equilibrium pair potential. This approach has the benefit that the par-

*Present address: Department of Applied Mathematics and Theoretical Physics, University of Cambridge, United Kingdom.
†david.grier@nyu.edu; URL: http://physics.nyu.edu/grierlab/

ticles' interactions are measured while the tweezers are extinguished, ensuring that the results are not contaminated by light-induced phenomena [21]. It also lends itself to measurements of dissimilar particle pairs [18]. "Blinking tweezer" measurements also require large data sets, however, and only work if the relaxation to equilibrium is free from kinematic effects, such as hydrodynamic coupling [24–27]. Demonstrating the absence of such artifacts is difficult.

Both long sampling times and nonequilibrium effects can be avoided by tracking the motions of particles trapped in optical tweezers. Accurate measurements of dynamic interactions, such as hydrodynamic coupling, can be extracted from observations of the coupled diffusion of particles individually trapped in optical tweezers [28,29]. Fast pair potential measurements can be realized by replacing the discrete optical tweezers with extended optical line traps [1,30–36], which allow trapped objects freedom of motion in one dimension. Appropriately sculpting the trap's one-dimensional force landscape optimizes statistical sampling [35]. Previous reports of line-trap interaction measurements have relied on separate calibrations of the lines' longitudinal potential energy landscape [37], and have accounted for light-induced interactions by extrapolating measurements at multiple laser powers to obtain the zero-power limit [34,35,38]. These calibrations and background measurements can be time-consuming and exacting, particularly if optical forces cannot be described simply, or if measuring optically induced interactions is one of the goals.

Using holographic methods to project line traps [1,7,39] and optimal statistical methods [6] to analyze the particles' trajectories addresses all of these issues. In particular, this combination eliminates the need for single-particle calibrations altogether and explicitly distinguishes particles' intrinsic interactions from one- and two-particle optically induced interactions. The result is a reliable, robust and, above all, rapid method for measuring colloidal interactions.

II. HOLOGRAPHIC LINE TRAPS

We project extended line tweezers using shape-phase holography [1] in the optimized [40] holographic optical trapping configuration [41,42]. Our system is built around an inverted optical microscope (Nikon TE2000U) with a 100 $\times$ oil-immersion objective (SPlanApo, NA 1.4). Light from a frequency-doubled $Nd:YVO_4$ laser (Coherent Verdi) is imprinted with phase-only holograms by a liquid crystal spatial light modulator (Hamamatsu X8267–16) before being brought to a focus by the objective. The same lens is used to form bright-field images on a charge coupled device (CCD) camera (NEC TI 324A II) at a system magnification of 135 nm/pixel. When used to project a shape-phase hologram encoding a line trap [1], this system brings the beam of light to a diffraction-limited focus as an anastigmatic conical wedge. The three-dimensional intensity distribution for such a trap is shown as a volumetric reconstruction [7] in Fig. 1(a). The line's image in the focal plane, shown in Fig. 1(b), has a half-width of 200 nm. The axial half-width is roughly three times larger, which also is consistent with diffraction-limited focusing. These intensity gradients establish the extended

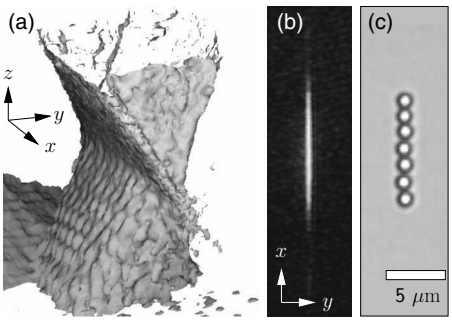

FIG. 1. Holographic optical line tweezer. (a) Isosurface enclosing 99% of the projected trap's intensity obtained from the volumetric reconstruction of a projected line trap. (b) Image of a line trap with a parabolic intensity profile, recorded in the focal plane. (c) Seven 1.5 μm diameter colloidal silica spheres dispersed in water and trapped along the line in three dimensions.

three-dimensional potential energy well within which colloidal particles can be captured. The image of 1.5 μm diameter colloidal silica spheres trapped along the line in Fig. 1(c) demonstrates the trap's ability to hold particles in three dimensions.

The line appears less bright at its ends because it is designed to have a parabolic intensity profile. Shaping the light's intensity along the focal line is useful for tuning the line tweezer's trapping characteristics [1,39]. Control over the line's intensity profile also can be used to mitigate imperfections due to aberrations and other defects in the optical train [43]. The stray light evident in the lower left corner of Fig. 1(a) results from such practical limitations.

Holographic line traps also can be combined with point-like holographic optical tweezers to select particular particles for measurement and to prevent others from intruding.

III. STATISTICAL MECHANICS OF COLLOIDAL PARTICLES ON A LINE TRAP

The potential energy landscape $\alpha v_1(\boldsymbol{x})$ that a particle experiences at position $\boldsymbol{x}$ along a line trap depends on the laser's power, α, as well as particle's properties and the line's characteristics. Scattered light also may induce inter-particle interactions, $\alpha v_2(\boldsymbol{x},\boldsymbol{y})$, that depend on laser power and on the particles' positions, $\boldsymbol{x}$ and $\boldsymbol{y}$, along the line. Contributions to this light-induced interaction include repulsive radiation pressure [34,36], optical binding forces [30,44], and optically induced changes in the particles' intrinsic interactions. It is reasonable to assume that these optical contributions to the system's free energy depend linearly on the laser power, α. By contrast, the particles' intrinsic pair potential, $u(r)$, should be independent of α. We assume that it depends only on the center-to-center separation, $r=|\boldsymbol{x}-\boldsymbol{y}|$.

Once particles are trapped on the line, they diffuse in the line's potential energy well with autocorrelation times set by viscous relaxation [29,40], which typically is less than 1 s for micrometer-diameter spheres. This also contrasts with measurements based on many-particle dynamics, which require long periods of equilibration [3].

The interacting particles' dynamics are dominated by random thermal fluctuations. Rather than studying their detailed

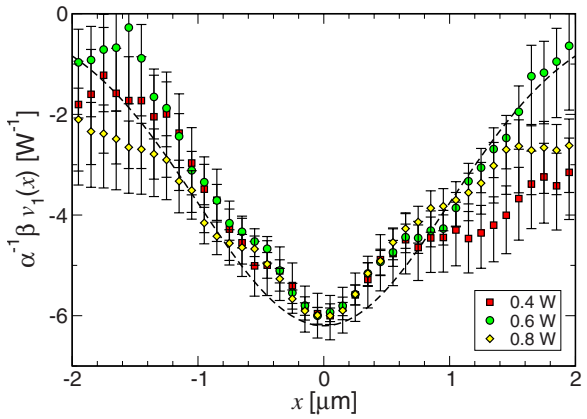

FIG. 2. (Color online) Measured potential energy profile, $v_1(x)$, for a 1.5 μm diameter silica sphere on a holographic line trap at three laser powers: α=0.4 W (squares), 0.6 W (circles), and 0.8 W (diamonds). Data are normalized by α for easier comparison.

trajectories, therefore, we measure the joint probability $P_2(\boldsymbol{x},\boldsymbol{y};\alpha)d\boldsymbol{x}d\boldsymbol{y}$ to find one particle within distance $d\boldsymbol{x}$ of $\boldsymbol{x}$ and the other within $d\boldsymbol{y}$ of $\boldsymbol{y}$. At equilibrium, this is related to the total potential energy,

$$w_\alpha(\boldsymbol{x},\boldsymbol{y}) = u(r) + \alpha[v_1(\boldsymbol{x}) + v_1(\boldsymbol{y}) + v_2(\boldsymbol{x},\boldsymbol{y})], \tag{1}$$

through the Boltzmann distribution

$$P_2(\boldsymbol{x},\boldsymbol{y};\alpha) = A_\alpha \exp[-\beta w_\alpha(\boldsymbol{x},\boldsymbol{y})], \tag{2}$$

where A_α is a power-dependent normalization and $\beta^{-1}=k_BT$ is the thermal energy scale at absolute temperature T. The joint probability can be measured by analyzing digital images of the trapped particles [2], taking care [5] to avoid imaging artifacts at small separations [4]. Inverting Eq. (2) then yields the total potential, $w_\alpha(\boldsymbol{x},\boldsymbol{y})$.

Extracting the intrinsic interaction, $u(r)$, from $w_\alpha(\boldsymbol{x},\boldsymbol{y})$ requires a way to account for the light-induced instrumental contributions, $v_1(\boldsymbol{x})$ and $v_2(\boldsymbol{x},\boldsymbol{y})$. Two approaches have been reported. The first [34] extrapolates measurements of $w_\alpha(\boldsymbol{x},\boldsymbol{y})$ performed at several laser powers to estimate $\lim_{\alpha\to 0} w_\alpha(\boldsymbol{x},\boldsymbol{y}) = u(r)$. The extrapolation is model-dependent, however, and requires several statistically well-sampled data sets to produce accurate results.

Alternatively, the single-particle contributions to $w_\alpha(\boldsymbol{x},\boldsymbol{y})$ can be calibrated by tracking a single particle's diffusion along the line before adding the second [37]. The resulting single-particle probability distribution, $P_1(\boldsymbol{x};\alpha)$, yields $v_1(\boldsymbol{x})$ through the Boltzmann distribution. The calibrated single-particle contributions then can be subtracted from the pair distribution function to yield an estimate for $u(r)$. The data plotted in Fig. 2 were obtained from one-dimensional projections of the measured single-particle probability distribution, $P_1(\boldsymbol{x};\alpha)$. As expected, the line's longitudinal profile, $v_1(x)$, is reasonably independent of laser power. These results were obtained with 2000 statistically independent samples at each laser power. Substantially more data would be required to sample the full three-dimensional single-particle distribution, $P_1(\boldsymbol{x};\alpha)$. Subtracting $\alpha[v_1(\boldsymbol{x})+v_1(\boldsymbol{y})]$ from $w_\alpha(\boldsymbol{x},\boldsymbol{y})$ leaves the optically induced pair interaction uncorrected. Although some reports find these contributions to be significant [34,36], others have found them to be negligibly weak [37] and have ignored them.

Rather than relying on extrapolations or calibrations to correct for light-dependent contributions to $w_\alpha(\boldsymbol{x},\boldsymbol{y})$, we explicitly scale them away by combining measurements at two laser powers, α_1 and α_2, through the relation

$$\frac{P_2^{\alpha_1/\alpha_2}(\boldsymbol{x},\boldsymbol{y};\alpha_2)}{P_2(\boldsymbol{x},\boldsymbol{y};\alpha_1)} = \exp\left(-\beta\left[\frac{\alpha_1}{\alpha_2}-1\right]u(r)\right). \tag{3}$$

Adequately sampling the two-dimensional distributions, $P_2(\boldsymbol{x},\boldsymbol{y};\alpha)$, still would require prohibitively large data sets. The intrinsic pair potential, however, depends only on the particles' separation. We therefore set $\boldsymbol{y}=\boldsymbol{x}+\boldsymbol{r}$ and formally average Eq. (3) over x and angles in $\boldsymbol{r}$ to obtain

$$\beta u(r) = \frac{\alpha_2}{\alpha_2-\alpha_1}\ln\left(\frac{\int P_2^{\alpha_1/\alpha_2}(\boldsymbol{x},\boldsymbol{x}+\boldsymbol{r};\alpha_2)d\boldsymbol{x}d\Omega_r}{\int P_2(\boldsymbol{x},\boldsymbol{x}+\boldsymbol{r};\alpha_1)d\boldsymbol{x}d\Omega_r}\right). \tag{4}$$

Equation (4) is useful only if an efficient method can be found to compute the integrals. Our approach is to treat each measurement $(\boldsymbol{x}_j,\boldsymbol{y}_j)$ of the particles' positions at time t_j as a discrete sample of the joint probability distribution, $P_2(\boldsymbol{x},\boldsymbol{y};\alpha)$ at power α. Given N_α such measurements, we compile the nonparametric density estimator [6],

$$\hat{P}_2(\boldsymbol{x},\boldsymbol{x}+\boldsymbol{r};\alpha) = \frac{1}{N_\alpha}\sum_{j=1}^{N_\alpha} K\left(\frac{\boldsymbol{x}_j-\boldsymbol{x}}{h(\boldsymbol{x}_j)}\right)K\left(\frac{\boldsymbol{y}_j-\boldsymbol{x}-\boldsymbol{r}}{h(\boldsymbol{y}_j)}\right), \tag{5}$$

which should converge to $P_2(\boldsymbol{x},\boldsymbol{y};\alpha)$ as the number of samples increases. The estimator's kernel, $K(\boldsymbol{x}/h)$, is a normalized non-negative integrable function and $h(\boldsymbol{x})$ is a smoothing parameter that varies adaptively with the density of experimentally sampled points. So long as $K(\boldsymbol{x}/h)$ is smooth and peaked at $K(0)$, its precise functional form is found to have little effect on $\hat{P}_2(\boldsymbol{x},\boldsymbol{y};\alpha)$ [6]. Consequently, we adopt

$$K\left(\frac{\boldsymbol{x}}{h}\right) = \frac{1}{\sqrt{2\pi}h}\exp\left(-\frac{x^2}{2h^2}\right), \tag{6}$$

using a width, h, that is adapted to the local density of experimentally sampled data points. Insufficient broadening yields needlessly noisy results; excessive broadening obscures features in $u(r)$. A reasonable estimate for the optimal adaptive sampling interval can be obtained by iterating

$$h(\boldsymbol{x}) = \left(\frac{4}{3N_\alpha}\right)^{1/5}\sqrt{\mathrm{var}[\hat{P}_2(\boldsymbol{x},\boldsymbol{x}+\boldsymbol{r};\alpha)]}, \tag{7}$$

where $\mathrm{var}[\hat{P}_2(\boldsymbol{x},\boldsymbol{x}+\boldsymbol{r};\alpha)]$ is the variance of the joint probability over the measured values of $\boldsymbol{r}$.

Using adaptive nonparametric density estimators to compute $\hat{P}_2(\boldsymbol{x},\boldsymbol{x}+\boldsymbol{r};\alpha)$ substantially accelerates convergence, and therefore minimizes the number of data points required to obtain a desired accuracy. Whereas the statistical error in histogram estimators for the projected one-dimensional prob-

ability density decreases with the number N of data points as $N^{-1/2}$, the error for the nonparametric estimator improves as $N^{-4/5}$ [45]. The potential, which scales as the logarithm of $\hat{P}_2(\boldsymbol{x},\boldsymbol{x}+\boldsymbol{r};\alpha)$, therefore also converges as $N^{-4/5}$.

The integrals in Eq. (4) usually have to be computed numerically. Given their dimensionality and the computational cost of evaluating the density estimator, Monte Carlo integration is a natural choice [46]. This approach is inherently more accurate than computing histograms of the particle positions because every data point contributes to the estimate for $u(r)$ without incurring the truncation errors inherent in binning. Multidimensional histogram estimators, furthermore, involve poorly controlled choices for the size, shape, placement, and orientation of the bins, all of which can substantially affect results. None of these considerations arise for adaptively optimized kernel estimators.

Although the numerical integrals in Eq. (4) are computationally intensive, they reduce the analysis to a one-dimensional form and thus greatly reduce the number of data points required to sample $u(r)$ accurately. Analytically factoring out the light-dependent interactions eliminates the need to calibrate the line-tweezer's potential energy well and greatly relaxes constraints on its functional form. In particular, we do not have to ensure that the trap implements a specific force profile such as a harmonic well. Instead, we require only that the particles can move along the line and that they sample interparticle separations over a specified range of interest. Colloidal interaction measurements based on Eqs. (4) and (5) are thus both optimally parsimonious with data and autocalibrating.

IV. EXPERIMENTAL DEMONSTRATION

We demonstrate our procedure by measuring the well-understood electrostatic interactions between micrometer-scale charge-stabilized colloidal silica spheres dispersed in deionized water. In this case, the electrostatic pair potential for two spheres of radius a each carrying effective charge Z^* [18,47,48] has the form [49]

$$\beta u(r) = Z^{*2}\lambda_B \frac{\exp(2\kappa a)}{(1+\kappa a)^2}\frac{\exp(-\kappa r)}{r}, \tag{8}$$

where $\lambda_B = e^2/(4\pi\epsilon k_B T)$ is the Bjerrum length in a medium of dielectric constant ϵ, and κ^{-1} is the Debye-Hückel screening length, given by $\kappa^2 = 4\pi\lambda_B n$ in a concentration n of monovalent ions. Previous measurements [2,16,18,21] have confirmed that Eq. (8) accurately describes the interactions between pairs of highly charged colloidal spheres provided they are kept far enough away from charged surfaces [5,12,13,18,19] or other spheres [14,15].

We performed measurements on two silica spheres of nominal diameter 1.53 μm (Bangs Laboratories 5303) dispersed in a 40 μm thick layer of water between a glass microscope slide and a No. 1.5 cover slip. Holographic characterization [50] reveals the mean diameter of the spheres in this sample to be $\sigma = 2a = 1.45 \pm 0.07$ μm. The edges of the coverslip were sealed to the surface of the slide with Norland Type 63 UV-cured adhesive to prevent evaporation. The glass surfaces were cleaned by oxygen plasma etching before assembly.

A holographic line trap $L = 8$ μm long was focused near the midplane of the sample volume far enough from the bounding surfaces to minimize their influence on the spheres' interactions. The line was designed to come to best focus uniformly in the microscope's focal plane, to have uniform phase along its length, and a Gaussian intensity profile [1]. Figure 2 shows the measured potential energy profile, which differs from the design by roughly 20%. Such variations would pose challenges if an accurate profile was required for our analysis. Because none of the spurious local potential energy wells is deep enough to trap a particle against thermal forces, however, deviations from the designed profile do not affect our measurement.

The curvature of the line's potential energy well was adjusted to bring the particles into proximity while still allowing them freedom of motion. Three 0.5 h data sets were obtained at laser powers of $\alpha = 0.4$, 0.6, and 0.8 W. The overall efficiency of our optical train is roughly 5%, taking into account the theoretical efficiency of the line-forming shape-phase hologram [1]. The total power projected onto each sphere at the highest power is of the order of 3 mW, which is comparable to conditions in conventional pointlike optical tweezers.

Thermal forces cause particles to wander away from the projected line. Although transverse in-plane root-mean-square (rms) fluctuations were no larger than 100 nm near the center of the line trap, and grew to no more than 200 nm at the ends, axial rms fluctuations were as large as 200 nm near the center and larger than 500 nm at the comparatively dim ends of the line. Equation (4) can be generalized to incorporate averages over the extra dimensions, with the appropriate redefinition of the interparticle separation r. The additional computational effort and substantial additional data required for multidimensional integrals would be burdensome, however. Instead, we pruned the data set to include only those measurements with single-particle axial excursions smaller than 200 nm. After this, just 2000 statistically independent measurements of the particles' positions were retained for each laser power, roughly 4% of the total number of frames acquired.

In future studies, off-line excursions can be minimized by using uniformly bright line traps whose force profiles are tailored with phase gradients [39]. This would greatly increase data retention rate and correspondingly reduce the measurement time required to acquire adequate statistics. Still further improvements in accuracy and efficiency could be obtained with the use of video holographic microscopy for precise three-dimensional particle tracking [50]. Acquiring data through conventional bright-field imaging on a parabolic line trap therefore should be considered a challenging test of the analytical methods that are the principal contributions of this work.

The pruned data were analyzed with Eqs. (4), (5), and (7) to obtain estimates for the intrinsic pair potential, which are plotted as points in Fig. 3. The results, plotted as circles in Fig. 3, are consistent with an energy resolution of $\pm 0.5 k_B T$ over a range of $25 k_B T$ and a spatial resolution of ± 20 nm, roughly twice the estimated uncertainty in the individual par-

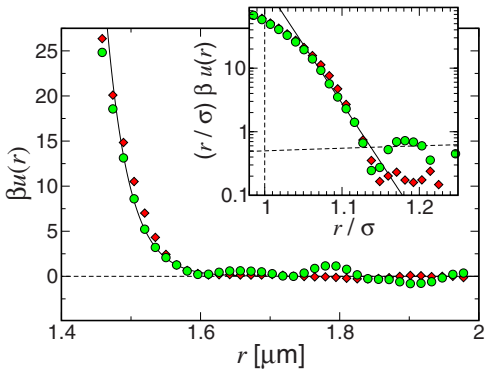

FIG. 3. (Color online) Measured pair potential for two 1.45 μm diameter colloidal silica spheres obtain with Eqs. (4)–(7) (circles) and by subtracting off single-particle optical contributions (diamonds). Inset: data replotted to facilitate comparison with Eq. (8). The dashed line indicates the estimated $0.5k_BT$ energy resolution of the measurement.

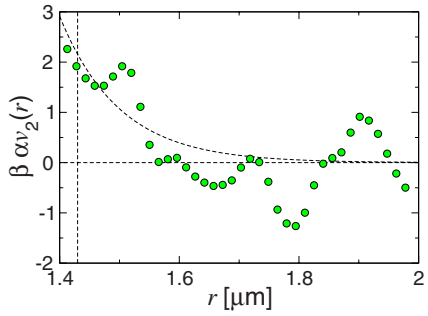

FIG. 4. (Color online) Position-averaged light-induced pair potential $\alpha v_2(r)$, at laser power $\alpha=0.4$ W, estimated from the data in Fig. 3.

ticles' positions. These results were obtained with the 0.6 and 0.8 W data sets. Quantitative agreement was obtained with other combinations of data sets. The upper range of accessible interaction energies is limited both by statistics and also by projection errors for particles very near contact.

Because the energy resolution at a given separation scales roughly linearly with the number of data points acquired at that separation [45] the time required to attain a desired resolution depends on the rate at which particles explore the available phase space along the line. This, in turn, depends on the particles' viscous relaxation time in the longitudinal trapping potential. By reducing the number of statistically independent data points required to achieve a given resolution, optimal statistical analysis reduces the number of viscous relaxation times that a measurement requires, and therefore can substantially reduce the duration of a measurement.

By making full use of the available data, optimal statistical analysis also eliminates the need for statistical oversampling to reduce round-off errors encountered in binning and bandwidth limitations encountered in power spectral analysis. Consequently, the present approach does not benefit particularly from high-speed data acquisition, and can be implemented with lower-cost equipment.

The inset to Fig. 3 shows the measured colloidal pair potential plotted for easy comparison with the prediction of Eq. (8). The observed linear trend is consistent with the anticipated screened Coulomb repulsion, and thus with previous measurements on similar colloidal particles under similar conditions [16,18,21]. The best-fit slope of this plot suggests a Debye-Hückel screening length of $\kappa^{-1}=32\pm10$ nm which is consistent with a $n=180$ μM total concentration of monovalent ions.

Based on the dissociation of terminal silanol groups with an estimated surface coverage of 6 nm^{-2}, the silica particles' effective charge number is anticipated [3] to be no larger than $Z^*\leq 6500$ and is known to be reduced by the presence of a neighboring sphere. The generalized [18] charge renormalization [47] result,

$$Z^* = \frac{e\zeta_0}{k_BT}\frac{a}{\lambda_B}(1+\kappa a), \tag{9}$$

relates the effective charge number to the effective surface potential, ζ_0. Taking $e\zeta_0=112$ meV yields $Z^*=5500$. The solid curve in Fig. 3 is the prediction of Eq. (8) for these values.

If we assume that there are no light-induced interactions, we can use the calibrated line profile to compute $u(r)$ from $P_2(\boldsymbol{x},\boldsymbol{x}+\boldsymbol{r};\alpha)$ directly. The results are plotted as diamonds in Fig. 3.

The difference between $u(r)$ computed in this way and that obtained from Eq. (4) is the one-dimensional projection of

$$\int P_1(\boldsymbol{x};\alpha)P_1(\boldsymbol{x}+\boldsymbol{r};\alpha)\alpha v_2(\boldsymbol{x},\boldsymbol{x}+\boldsymbol{r})d\boldsymbol{x}d\Omega_r \approx \alpha v_2(\boldsymbol{r}), \tag{10}$$

which provides at least a rough estimate for the light-induced interaction between the two spheres. For $\alpha=0.4$ W, the result is consistent with a short-ranged exponential repulsion with a decay length of 80 nm (see Fig. 4). Such an optically induced repulsive interaction is consistent with previous studies of multiple colloidal particles on extended optical traps [34]. Presumably, light scattered by one sphere impinges on its neighbor and gives rise to radiation pressure. In this interpretation, the range of the repulsion is set by the nontrivial angular distribution of the Lorenz-Mie scattered light [51].

Peaks in $v_2(r)$ might be due to power-dependent changes in the functional form of $v_1(\boldsymbol{x})$. Such changes can be seen in the single-particle potentials in Fig. 2 and might therefore explain the peaks in the estimate for $u(r)$ at $r=1.66$ and 1.79 μm in Fig. 3.

Alternatively, structure in $v_2(r)$ could arise from interference between the two spheres' scattering patterns. In this case, the results in Fig. 4 would constitute new experimental evidence for longitudinal optical binding [30,44]. It should be emphasized, however, that these features are barely resolved over the estimated $1k_BT$ error in $v_2(r)$.

Distinguishing optical binding from power-dependent artifacts is made difficult in this data set by the line trap's parabolic intensity profile. Measurements in uniformly bright

line traps with phase-gradient longitudinal potential wells are under way and will be reported elsewhere.

Regardless of the interpretation of $v_2(r)$, ignoring optically induced pair interactions would lead to subtle systematic errors in estimates for the intrinsic pair interaction, $u(r)$. In particular, the result for $u(r)$ obtained by applying single-particle calibrations overestimates the repulsive force at small separations. The principal consequence for the present system would be to systematically overestimate the particles' effective charge number.

The apparent absence of light-induced interactions between particles trapped on scanned line tweezers [37] may be ascribed to the smaller size of the silica particles in that study. Whereas the Mie scattering pattern for 1.5 μm diameter silica spheres at a vacuum wavelength of 532 nm includes a sizable in-plane component, 1 μm diameter spheres scatter virtually all light at 488 nm into the forward direction [50,51]. No optically induced interaction should be expected unless spheres scatter light toward their neighbors.

The electrostatic interactions between isolated pairs of colloidal spheres far from surfaces are very well-understood. The agreement between experiment and theory in this model system demonstrates that the protocol described above can be applied with reasonable confidence to systems whose underlying interactions are less well-understood.

V. CONCLUSION

We have described and demonstrated a method for measuring colloidal pair interactions based on particles' equilibrium statistics in an extended optical trap. This method is self-calibrating in the sense that no *a priori* information regarding the trap's effective potential energy landscape is required to measure trapped particles' interactions. This offers an advantage in both time and effort over previously described methods, which require separate single-particle calibrations of the trapping potential.

Our method makes good use of the flexible reconfigurability of holographic trap projection through shape-phase holography. The same analytical technique also can be applied to line tweezers created with cylindrical lenses, or through rapid scanning.

Optimizing the transverse stiffness of the trap, particularly in the axial direction, can substantially improve data retention efficiency and thereby reduce measurement duration. The ultimate limit on measurement speed is set, however, by the particles' viscous relaxation rate in the line tweezer. This also can be optimized through holographic control over the potential energy well's shape. The use of optimal statistical analysis then minimizes the number of viscous relaxation times required for adequate statistical sampling.

Combining optical micromanipulation, digital video microscopy, and optimal statistical analysis offers an efficient and effective method to probe colloidal interactions. The method described here is easily generalized for dissimilar pairs of particles. Even more appealing is the possibility of performing multiple simultaneous measurements by projecting multiple holographic line traps. This opens up the possibility of using colloidal interaction measurements for process control and quality assurance testing.

ACKNOWLEDGMENTS

This work was supported by the National Science Foundation through Grant No. DMR-0606415 and through the support of the Keck Foundation.

[1] Y. Roichman and D. G. Grier, Opt. Lett. **31**, 1675 (2006).
[2] J. C. Crocker and D. G. Grier, J. Colloid Interface Sci. **179**, 298 (1996).
[3] S. H. Behrens and D. G. Grier, Phys. Rev. E **64**, 050401(R) (2001).
[4] J. Baumgartl and C. Bechinger, Europhys. Lett. **71**, 487 (2005).
[5] M. Polin, D. G. Grier, and Y. Han, Phys. Rev. E **76**, 041406 (2007).
[6] B. W. Silverman, *Density Estimation for Statistics and Data Analysis* (Chapman and Hall, New York, 1992).
[7] Y. Roichman, I. Cholis, and D. G. Grier, Opt. Express **14**, 10907 (2006).
[8] T. Savin and P. S. Doyle, Phys. Rev. E **71**, 041106 (2005).
[9] G. M. Kepler and S. Fraden, Phys. Rev. Lett. **73**, 356 (1994).
[10] M. D. Carbajal-Tinoco, F. Castro-Román, and J. L. Arauz-Lara, Phys. Rev. E **53**, 3745 (1996).
[11] H. Acuña-Campa, M. D. Carbajal-Tinoco, J. L. Arauz-Lara, and M. Medina-Noyola, Phys. Rev. Lett. **80**, 5802 (1998).
[12] Y. Han and D. G. Grier, Phys. Rev. Lett. **92**, 148301 (2004).
[13] Y. Han and D. G. Grier, J. Chem. Phys. **122**, 064907 (2005).
[14] M. Brunner, C. Bechinger, W. Strepp, V. Lobaskin, and H. H. von Grunberg, Europhys. Lett. **58**, 926 (2002).
[15] C. Russ, M. Brunner, C. Bechinger, and H. H. Von Grunberg, Europhys. Lett. **69**, 468 (2005).
[16] K. Vondermassen, J. Bongers, A. Mueller, and H. Versmold, Langmuir **10**, 1351 (1994).
[17] R. V. Durand and C. Franck, Phys. Rev. E **61**, 6922 (2000).
[18] J. C. Crocker and D. G. Grier, Phys. Rev. Lett. **77**, 1897 (1996).
[19] Y. Han and D. G. Grier, Phys. Rev. Lett. **91**, 038302 (2003).
[20] A. Ashkin, J. M. Dziedzic, J. E. Bjorkholm, and S. Chu, Opt. Lett. **11**, 288 (1986).
[21] J. C. Crocker and D. G. Grier, Phys. Rev. Lett. **73**, 352 (1994).
[22] S. H. Behrens, J. Plewa, and D. G. Grier, Eur. Phys. J. E **10**, 115 (2003).
[23] S. K. Sainis, V. Germain, and E. R. Dufresne, Phys. Rev. Lett. **99**, 018303 (2007).
[24] A. E. Larsen and D. G. Grier, Nature (London) **385**, 230 (1997).
[25] E. R. Dufresne, T. M. Squires, M. P. Brenner, and D. G. Grier, Phys. Rev. Lett. **85**, 3317 (2000).
[26] T. M. Squires and M. P. Brenner, Phys. Rev. Lett. **85**, 4976 (2000).
[27] T. M. Squires, J. Fluid Mech. **443**, 403 (2001).
[28] J. C. Meiners and S. R. Quake, Phys. Rev. Lett. **82**, 2211

(1999).
[29] M. Polin, D. G. Grier, and S. R. Quake, Phys. Rev. Lett. **96**, 088101 (2006).
[30] M. M. Burns, J.-M. Fournier, and J. A. Golovchenko, Phys. Rev. Lett. **63**, 1233 (1989).
[31] A. E. Chiou, W. Wang, G. J. Sonek, J. Hong, and M. W. Berns, Opt. Commun. **133**, 7 (1997).
[32] K. Sasaki, M. Koshio, H. Misawa, N. Kitamura, and H. Masuhara, Opt. Lett. **16**, 1463 (1991).
[33] L. P. Faucheux and A. J. Libchaber, Phys. Rev. E **49**, 5158 (1994).
[34] J. C. Crocker, J. A. Matteo, A. D. Dinsmore, and A. G. Yodh, Phys. Rev. Lett. **82**, 4352 (1999).
[35] P. L. Biancaniello, A. J. Kim, and J. C. Crocker, Phys. Rev. Lett. **94**, 058302 (2005).
[36] P. L. Biancaniello and J. C. Crocker, Rev. Sci. Instrum. **77**, 113702 (2006).
[37] M. Brunner, J. Dobnikar, H. H. von Grunberg, and C. Bechinger, Phys. Rev. Lett. **92**, 078301 (2004).
[38] R. J. Owen, J. C. Crocker, R. Verma, and A. G. Yodh, Phys. Rev. E **64**, 011401 (2001).
[39] Y. Roichman, B. Sun, Y. Roichman, J. Amato-Grill, and D. G. Grier, Phys. Rev. Lett. **100**, 013602 (2008).
[40] M. Polin, K. Ladavac, S.-H. Lee, Y. Roichman, and D. G. Grier, Opt. Express **13**, 5831 (2005).
[41] E. R. Dufresne and D. G. Grier, Rev. Sci. Instrum. **69**, 1974 (1998).
[42] D. G. Grier, Nature (London) **424**, 810 (2003).
[43] Y. Roichman, A. S. Waldron, E. Gardel, and D. G. Grier, Appl. Opt. **45**, 3425 (2006).
[44] M. M. Burns, J.-M. Fournier, and J. A. Golovchenko, Science **249**, 749 (1990).
[45] J. R. Thompson and R. A. Tapia, *Nonparametric Function Estimation, Modeling, and Simulation* (SIAM, Philadelphia, 1990).
[46] G. S. Fishman, *Monte Carlo: Concepts, Algorithms, and Applications* (Springer, New York, 1995).
[47] S. Alexander, P. M. Chaikin, P. Grant, G. J. Morales, P. Pincus, and D. Hone, J. Chem. Phys. **80**, 5776 (1984).
[48] E. Trizac, Phys. Rev. E **62**, R1465 (2000).
[49] W. B. Russel, D. A. Saville, and W. R. Schowalter, *Colloidal Dispersions, Cambridge Monographs on Mechanics and Applied Mathematics* (Cambridge University Press, Cambridge, England, 1989).
[50] S.-H. Lee, Y. Roichman, G.-R. Yi, S.-H. Kim, S.-M. Yang, A. van Blaaderen, P. van Oostrum, and D. G. Grier, Opt. Express **15**, 18275 (2007).
[51] C. F. Bohren and D. R. Huffman, *Absorption and Scattering of Light by Small Particles* (Wiley, New York, 1983).